Reentrant rigidity percolation in structurally correlated filamentous networks

Jonathan Michel [1,*] Gabriel von Kessel [1] Thomas Wyse Jackson,[2]
Lawrence J. Bonassar,[3,4] Itai Cohen,[2] and Moumita Das [1,†]
[1]*School of Physics and Astronomy, Rochester Institute of Technology, Rochester, New York 14623-5603, USA*
[2]*School of Physics, Cornell University, Ithaca, New York 14853, USA*
[3]*Meinig School of Biomedical Engineering, Cornell University, Ithaca, New York 14853, USA*
[4]*Sibley School of Mechanical and Aerospace Engineering, Cornell University, Ithaca, New York 14853, USA*

(Received 24 April 2022; accepted 25 October 2022; published 30 November 2022)

Many biological tissues feature a heterogeneous network of fibers whose tensile and bending rigidity contribute substantially to these tissues' elastic properties. Rigidity percolation has emerged as an important paradigm for relating these filamentous tissues' mechanics to the concentrations of their constituents. Past studies have generally considered tuning of networks by spatially homogeneous variation in concentration, while ignoring structural correlation. We introduce here a model in which dilute fiber networks are built in a correlated manner that produces alternating sparse and dense regions. Our simulations indicate that structural correlation consistently allows tissues to attain rigidity with less material. We further find that the percolation threshold varies nonmonotonically with the degree of correlation, such that it decreases with moderate correlation and once more increases for high correlation. We explain the eventual reentrance in the dependence of the rigidity percolation threshold on correlation as the consequence of large, stiff clusters that are too poorly coupled to transmit forces across the network. Our study offers deeper understanding of how spatial heterogeneity may enable tissues to robustly adapt to different mechanical contexts.

DOI: 10.1103/PhysRevResearch.4.043152

I. INTRODUCTION

Networks and networklike structures are ubiquitous in biological cells and tissues and provide the basis for their mechanical properties and functions. Biopolymer networks are largely responsible for the mechanical response of the cytoskeleton of cells [1–6] and the extracellular matrix of tissues [7–11]; more recently, rigidly percolating connected networks of cells have been shown to account for the viscoelasticity of developing embryos [12]. These networks are generally highly disordered and spatially inhomogeneous as a result of how they are assembled and disassembled. For example, cytoskeletal networks are highly dynamic and have a complex and heterogeneous spatial organization allowing for context-dependent cell remodeling and response [1]. As a second example, the collagen II scaffold in articular cartilage is densest in the vicinity of chondrocytes, cells which secrete extracellular matrix material to construct and sustain collagen networks [13]. In fact, previous work has established spatial heterogeneity as a crucial consideration in developing faithful cartilage replacements and scaffolds for tissue regeneration [14,15].

In the past two decades, there has been extensive study of disordered biopolymer networks through *in vitro* experiments and simulations, which have provided a wealth of information about these networks' responses to mechanical stimuli [16–24]. To date, however, almost all computational studies of biopolymer networks have focused on spatially homogeneous systems and ignored the presence of structural correlations, which can have significant consequences for the collective properties of the network.

The effects of heterogeneity and correlations have been investigated in other percolation phenomena, such as colloidal gelation [25] and connectivity percolation arising from the union of random walks [26]. Heterogeneity has also been found to be consequential in determining the mechanics of glassy solids [27] and to cause a shift in the critical temperature at which various critical phenomena occur [28]. Nonetheless, to our knowledge, the role of spatial heterogeneity in the mechanics of fibrous tissues has yet to be systematically explored. Here, we address this gap and present a novel investigation of the percolation of rigidity in structurally correlated fiber networks, which are found in many cells and tissues, using a lattice-based framework.

Lattice-based fiber networks are a prominent paradigm for modeling biopolymer scaffolds [19,21,22,24,29]. These networks are constructed by laying down infinitely long fibers in a regular pattern, such that whenever two fibers cross, there is a crosslink which allows free rotation of the fibers but does not allow them to slide. The fibers can stretch and bend, but

*Corresponding author should be addressed: jamsps@rit.edu
†Corresponding author should be addressed: modsps@rit.edu

pay energy penalties for these deformations. Each fiber can further be thought of as a collinear series of connected bonds, such that random removal of bonds yields a broad distribution of fiber lengths.

The mechanical response of such a disordered fiber network can be mapped to the fraction of bonds present. Starting with a network in which all the bonds are present, one can progressively decrease network rigidity by removing bonds. Once the network reaches a certain threshold of bond occupation, its elastic moduli undergo a dramatic, many-decade decrease, dropping to negligibly small values. This mechanical phase transition is known as rigidity percolation [19,29]. This phenomenon is distinct from connectivity percolation, which requires only the existence of a path from one edge of the network to another. In general, a network with a system-spanning connected component may not be able to transmit force from one boundary to another. Dilute fiber networks have shown great promise as micromechanical models for *in vitro* cytoskeletal networks [16–19], and more recently for extracellular matrix networks in tissues [8,11,30].

Previous computational studies of fiber networks have examined spatially homogeneous disordered networks, in which bonds are excluded or retained purely at random, and have not considered the possibility of correlations in the inclusion of bonds [16,17,19–21]. In this paper we introduce a model in which bonds are added in a structurally correlated manner to account for the pronounced heterogeneity in the distribution of material observed in cells and tissues. In this model, the likelihood of adding a bond is contingent upon the number of adjacent bonds already present. This protocol gives rise to networks in which already dense regions become further enriched with material, while sparse regions remain comparatively dilute.

II. MODEL

A. Network construction

As we are interested in biopolymer networks in which vertices correspond to crossings of adjacent filaments, we choose as our model network the kagome lattice [8], with a maximum coordination number of 4. We adjust the elastic moduli of networks by randomly retaining a subset of the bonds, such that some portion, p, is included. In the absence of structural correlation, p corresponds to the probability that each bond is retained, such that there is an independently and identically distributed probability of keeping each bond. We instead use the term bond portion to reflect the fact that, for correlated dilute networks, once the network is seeded with an initial set of bonds, other bonds do not have an identical likelihood of inclusion.

We employ an iterative process, introduced in [25], in which, at each step, a candidate bond is chosen at random from those bonds that have not yet been included in the network. We then count the number of bonds adjacent to the candidate bond n_a that have already been retained, where adjacency is defined by the condition that two bonds share a common vertex. For the kagome lattice, the maximum possible number of adjacent bonds, $n_{a,\max}$, is 6. Given a correlation strength, c, where $0 \leqslant c < 1$, the candidate bond is added with a probability

$$P = (1-c)^{n_{a,\max}-n_a}, \tag{1}$$

where $c = 0$ corresponds to a purely random dilution and $c \approx 1$ corresponds to a maximally correlated dilution, in which a bond is rejected unless all adjacent bonds have been retained. This process is repeated until the desired portion of bonds has been retained.

In Fig. 1, we show representative samples of networks with varying degrees of dilution and correlation, including no correlation. Increasing the correlation strength for a given bond portion yields a network with dense clusters, interspersed with sparse regions. As further bonds are added, relatively dense regions become more enriched with material, while voids between these regions persist until the bond portion approaches 1. Notably, our procedure for adding structural correlation is isotropic, so that it does not confer long-range orientational order, apart from that arising due to the discrete rotational symmetry of the kagome lattice.

The data presented in the main text were computed using networks occupying an approximately square region with a side length of about 330 bond lengths. Such networks contain approximately 200 000 bonds when all bonds are present. We have also considered two other cases in which networks have approximately 800 000 and 2 000 000 bonds, respectively, in the fully connected state, to check for finite size effects, and found substantially similar results. Details of the finite size effect study may be found in Appendix C.

B. Mechanical model

The bonds of the network resist stretch and compression with a Hookean spring stiffness, α, and resist bending with a bending rigidity, κ. Bending resistance is implemented by regarding adjacent, collinear bonds as consecutive segments of a fiber. If the bond connecting vertices i and j is collinear with and adjacent to the bond joining vertices j and k, then we penalize a change in the angle $\angle ijk$ by an amount proportional to the square of the angular deflection.

We focus on the mechanical response in the linear response regime, so that the deformation energy consists of terms quadratic in the strain. Following [8], we truncate the deformation energy to leading order in the displacement of vertices from the reference configuration of the network and model the energy as

$$E_{\text{strain}} = \frac{\alpha}{2}\sum_{\langle ij\rangle} p_{ij}(\mathbf{u}_{ij}\cdot\hat{\mathbf{r}}_{ij})^2 + \frac{\kappa}{2}\sum_{\langle ijk\rangle} p_{ij}p_{jk}[(\mathbf{u}_{ji}+\mathbf{u}_{jk})\times\hat{\mathbf{r}}_{ji}]^2. \tag{2}$$

Here, $\langle ij\rangle$ denotes a sum over pairs of vertices sharing a bond, $\langle ijk\rangle$ denotes a sum over vertices of adjacent, collinear bonds, and p_{ij} is defined to be 1 if the bond between bonds i and j is retained and 0 otherwise. Further, $\mathbf{u}_{ij}$ denotes the difference between the displacement vectors for vertices i and j, and $\hat{\mathbf{r}}_{ij}$ denotes the direction vector of the bond between vertices i and j in the reference state.

Note that, while we penalize filament stretching and filament bending, there is no energy cost of changing the angle between crossing filaments at a crosslink. In such fiber

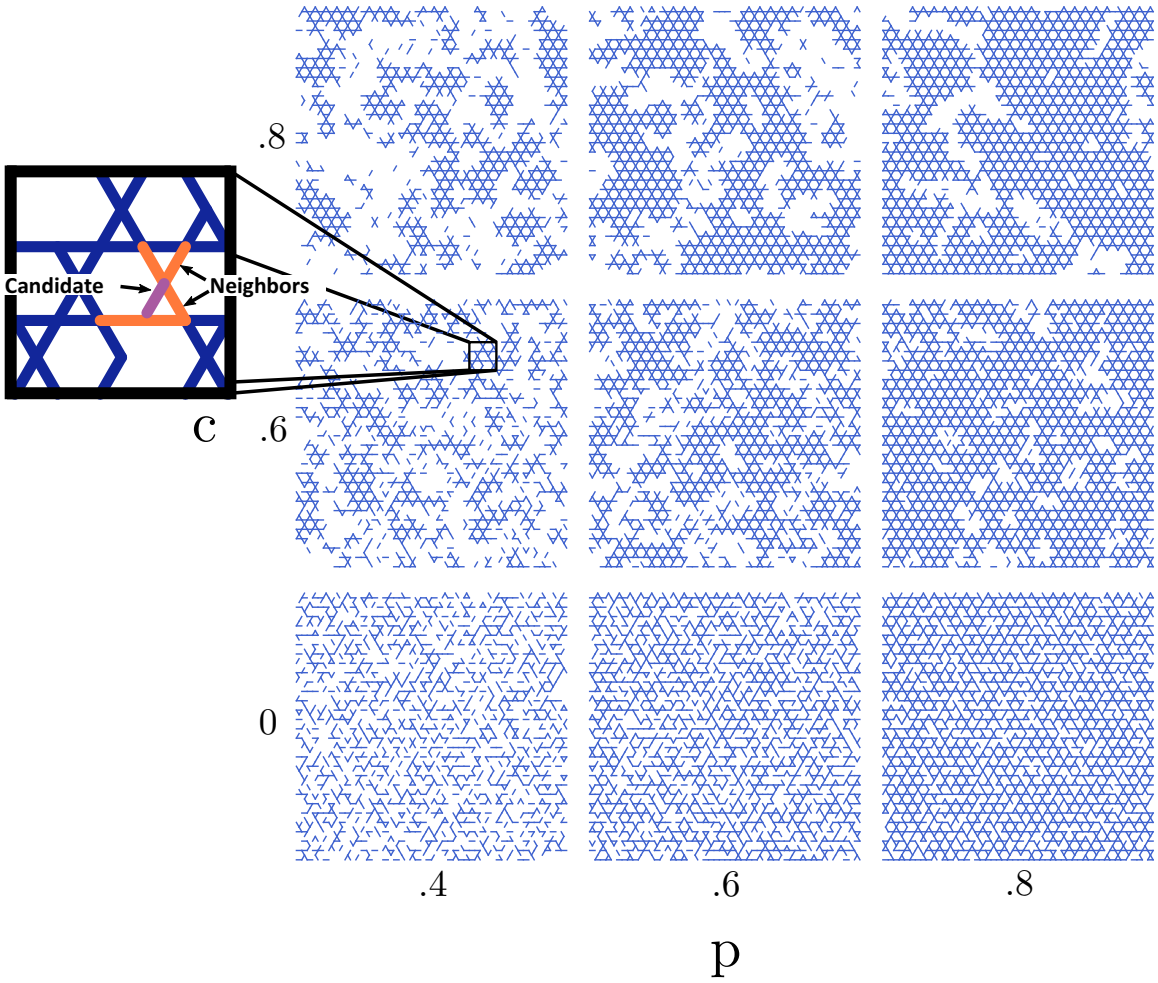

FIG. 1. Sample networks are shown in which correlation strength is varied from 0 to 0.8 and the bond portion is varied from 0.4 to 0.8. We show a magnified inset at the left of the figure to illustrate the correlated construction process. A candidate, marked in magenta, is considered for inclusion and has five neighbors, marked in orange. As the correlation strength is increased, networks transition from arrangements of homogeneously dispersed bonds to networks with dense clusters interspersed with sparse voids. Our procedure for adding structural correlation thus adds strong density fluctuations, without introducing long-range orientational order.

networks, in which bending forces couple only collinear, adjacent bonds, the rigidity percolation threshold has been found to be higher than the connectivity percolation threshold. The rigidity and connectivity percolation thresholds were found to be equal if every pair of adjacent bonds is coupled by bending forces [22].

C. Structural relaxation procedure

We simulate the shear mechanics of our model networks by imposing a series of small, simple shear displacements of the vertices at the top. The displacements of the vertices at the bottom of the network are constrained to be zero, while along the sides we impose periodic boundary conditions. Given these constraints, we minimize the energy given in (2) for a small strain, $\epsilon_s = 0.001$, and compute the shear modulus according to the relation

$$E = \frac{1}{2} A G \epsilon_s^2, \tag{3}$$

where E is the minimized energy, A is the area of the network, and G is the shear modulus. In seeking a mechanical ground state, we choose as our starting guess an affine displacement field, in which the displacement of each vertex is given by a global linear transformation. For the simple shear we apply to our networks, this amounts to displacing a point (x, y) by

$$\vec{u}(x, y) = [\epsilon_s (y - y_{\min}), 0], \tag{4}$$

where $\vec{u}$ is the displacement field, ϵ_s is the shear strain, and $y_{\min}$ is the minimum y coordinate of any vertex in the network. Full details of this calculation may be found in Appendix A.

III. RESULTS AND DISCUSSION

A. Shear mechanics

We first examined how the rigidity percolation threshold can be tuned by varying the degree of correlation. We considered nine distinct values of c, ranging from 0 to 0.8, in steps of 0.1, and 61 distinct values of p, ranging from 0.4 to 1, in steps of 0.01. We carried out structural relaxation for 10 realizations for each combination of c and p, and identified G for each combination as the geometric mean of the 10 values. The shear modulus G, normalized by its universal maximum, G_0,

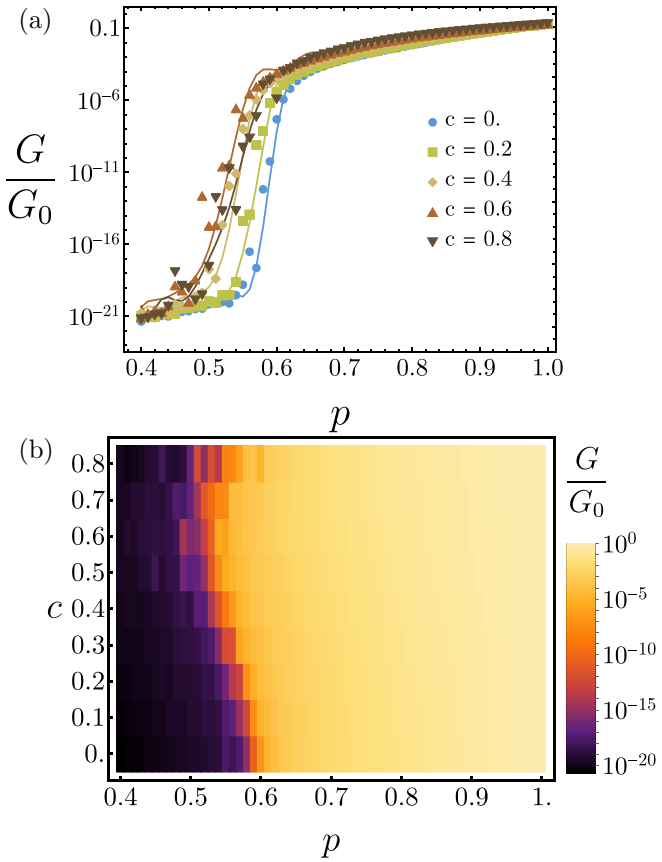

FIG. 2. In panel (a), we show the scaling of shear modulus with bond portion for several structural correlation strengths. While the dependence of the shear modulus on the bond portion is qualitatively similar in each case, the point of rigidity percolation shifts initially to the left, then back to the right with increasing structural correlation. In panel (b), we show the dependence of G on c and p for the full range of parameter space considered. The reentrance of the dependence of p_c on structural correlation strength is clearly discernible in a contour of marginal stiffness on the left side of the heat map. We attribute this reentrance to two competing effects: the need for rigid clusters and the need for strong coupling between adjacent clusters.

is shown vs p for several values of c in Fig. 2(a), accompanied by a full phase diagram in Fig. 2(b).

Figures 2(a) and 2(b) provide the first indications of an intriguing variation in the rigidity percolation threshold with the degree of correlation c of the disordered network. For each value of c, we find a qualitatively similar scaling of the shear modulus with the bond fraction. Interestingly, however, the rigidity percolation threshold, i.e., the critical bond fraction, p_c, at which the shear modulus first differs appreciably from zero, shifts markedly and nonmonotonically as c is varied: while introducing a moderate correlation strength initially diminishes p_c, this effect saturates at about $c = 0.6$ and p_c increases for still larger values of c.

To quantitatively identify the rigidity percolation threshold for each value of c, we considered pairs of bond fraction and shear modulus for which the shear modulus ranged from 10^{-9} to $\sim 10^{-2}$. This ensured that the shear modulus was greater than machine or algorithmic error, but still small in comparison with its maximal value, G_0, at $p = 1$. We used the method of least squares to fit each set of bond fraction-shear modulus pairs to a power law of the form

$$G = k(p - p_c)^{\beta}. \tag{5}$$

For each value of c, we found a good fit to Eq. (5) over at least seven decades of dynamic range in the shear modulus. In each case, the correlation coefficient, R^2, between $\log_{10}(G)$ and $\log_{10}[k(p - p_c)^{\beta}]$ is $\geqslant 0.96$. For the homogeneous case $c = 0$, we recover the previously established result of $p_c \approx 0.6$ [31].

As shown in Fig. 3(a), in which p_c is plotted vs c, our power law fits affirm the trend in p_c previously identified by inspection in Fig. 2. Surprisingly, the scaling exponent, β, on the other hand, exhibits the opposite trend, increasing with c until about $c = 0.6$, and decreasing thereafter. This dependence of β on c indicates that an earlier onset of rigidity percolation is accompanied by a more abrupt rise in the shear modulus at the point of percolation.

As shown in Fig. 3(c), we find β to decrease linearly with p_c ($R^2 = 0.92$). We attribute the decrease in β with p_c to two competing factors determining percolation: the presence of large, rigid clusters and sound mechanical coupling of adjacent clusters. As the correlation strength is increased beyond its optimum value, the network segregates into large, dense regions that are too poorly connected to enable optimal transmission of stress. The optimal correlation strength of 0.6 strikes an ideal balance, enabling the greatest gain in stiffness per unit material. To substantiate this conjecture, we turn to detailed analysis of network displacement fields.

B. Analysis of nonaffine deformation

To gain further insight into the micromechanical mechanisms underlying the reentrance in the rigidity percolation threshold, we quantified the degree of nonaffinity in each network. Nonaffinity quantifies the departure of a displacement field of a strained material from the displacement expected in a simple, homogeneous elastic continuum. In an affinely deforming network subjected to simple shear, a vertex with an initial location $\vec{r}_0 = (x_0, y_0)$ will be mapped to the final location $\vec{r}'_A = (x_0 + \epsilon_s y_0, y_0)$, where ϵ_s is the shear strain. The nonaffine displacement field $\vec{u}_{NA}$ is defined as $\vec{r}\,' - \vec{r}'_{NA}$, where $\vec{r}\,'$ is the true displacement field. The nonaffine parameter, Γ, is then defined as

$$\Gamma = \frac{1}{N\epsilon_s^2 l_0^2} \sum_{i=1}^{N} |\vec{u}_{NA}|^2, \tag{6}$$

where l_0 is the length of an undeformed bond and N is the number of vertices in the network [32]. Nonaffinity is a well established means of characterizing the difference in behavior of a purely entropic rubber and a gel of semiflexible polymers [24] and has been found more broadly to be important in accounting for the shear mechanics of disordered solids [33]. We computed Γ for all ten network realizations for each combination of p and c and calculated the final nonaffine parameter as the arithmetic mean over all realizations.

We note that, owing to zero frequency modes in the stiffness matrices of underconstrained networks for which $p < p_c$, there will be some ambiguity in the solution for the displacement field. This ambiguity is not entirely lifted by the constraints we impose at the boundaries. While the nonaffine

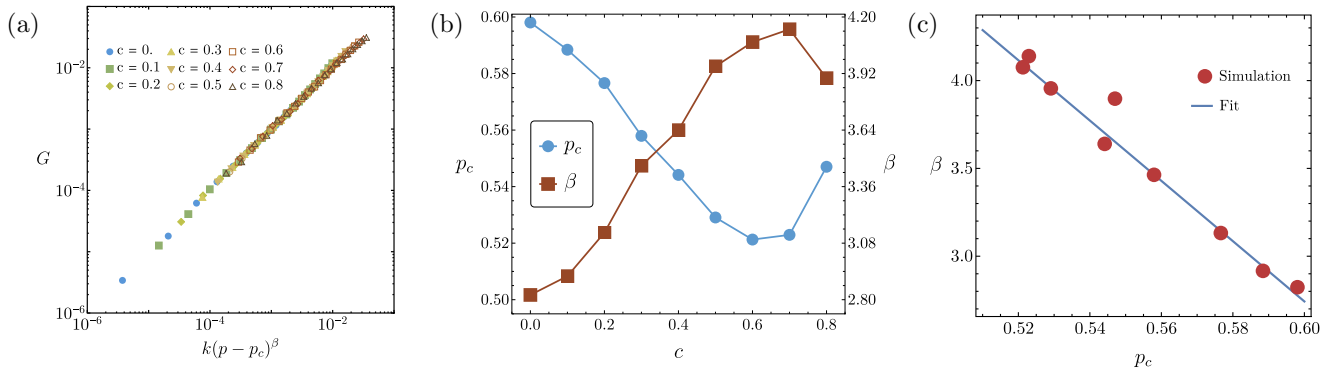

FIG. 3. Scaling behavior near the rigidity threshold: In (a), we show the results of fitting shear modulus–bond portion pairs to Eq. (5). In each case, we find a sound fit spanning six to seven decades in the shear modulus. In (b), we show fitting results for the critical bond portion, p_c, and the scaling exponent, β, of the shear modulus with the excess bond portion. The scaling exponent exhibits the opposite trend from the critical bond portion, indicating that a low percolation threshold is accompanied by a more abrupt increase in the shear modulus. In (c), we demonstrate that the critical bond portion is a reliable predictor of the critical exponent relating growth in the shear modulus to the excess bond portion. We find that the value $c = 0.6$ yields an optimal trade-off between a need for large, rigid clusters and a need for sound mechanical coupling of adjacent clusters to enable coordinated, system-spanning force propagation. For excessive correlation, dense clusters amount to stiff inclusions in an otherwise undercoordinated network.

parameter for $p < p_c$ is therefore protocol dependent, we argue that it is still illuminating in this regime. Our trial solution of affine displacement would be exact if our networks had completely homogeneous mechanical response, but this guess fails for the heterogeneous networks we consider here. Nonaffine deformations generically result from an imbalance of forces in the affinely deformed state [32,34]. A large departure of the displacement field from our starting affine guess thus reveals a high degree of mechanical heterogeneity. In a similar vein, previous work has found nonaffine rearrangements to be useful in identifying "soft spots" in which the onset of plasticity is most likely in disordered granular media [35,36].

As reported in previous studies [21,24], we find a pronounced peak in the nonaffine parameter near the rigidity percolation threshold, as shown in Fig. 4(a). The relatively small values of the nonaffine parameter for $p \ll p_c$ and $p \gg p_c$ are reasonable, as, in these limits, all parts of the network are either equally soft or equally stiff, respectively. While the same general trend holds for all correlation strengths, the peak in the nonaffine parameter becomes lower and broader as the structural correlation strength is increased. We posit that this peak broadening is associated with the formation of local rigid regions, joined by weakly connected interstitial regions, such that stress is distributed in a nonuniform manner over a larger range of bond fractions for networks with high structural correlation. We investigate this idea further by considering the spatial correlations in the nonaffine displacement field.

We first consider a radial nonaffine correlation function, $g(r)$. We take the inner product of nonaffine displacements for all pairs of points within some cutoff distance, r_{cut}, of one another and bin displacement vectors between pairs of points into annular sectors of thickness Δr. We then define $g(r)$ as

$$g(r) = \frac{1}{\langle |\vec{u}_{NA}|^2 \rangle} \times \langle \vec{u}_{NA}(\vec{r}_i) \cdot \vec{u}_{NA}(\vec{r}_j) \rangle_{r \leqslant |\vec{r}_j - \vec{r}_i| < r + \Delta r}, \quad (7)$$

where the first average runs over all points and the second average runs over all distinct pairs of points i, j such that the positions of vertices i and j in the undeformed lattice are separated by a distance in the range $[r, r + \Delta r)$. This normalizes $g(r)$ to be equal to 1 when $r = 0$.

For each combination of p and c, we find $g(r)$ to be well fit (for all cases, $R^2 \geqslant 0.98$) by the form

$$g(r) = 1 + a(e^{-r/\lambda} - 1). \quad (8)$$

We show a representative set of curves in Fig. 4(b), for $c = 0.6$ and varying bond fractions. Symbols indicate data points, while lines are fits to Eq. (8). Initially, the floor of $g(r)$ decreases, reaching its lowest point near the rigidity percolation threshold, then steadily increases for larger values of p. We attribute the early decrease in the floor to incipient rigid clusters that deform differently from the surrounding soft regions, such that there is no coordinated, long-range force transmission. The subsequent rise in the minimum of $g(r)$ is associated with the emergence of system-wide spanning force chains beyond the rigidity percolation threshold.

From the decay distance, λ, in Eq. (8), we infer an effective mechanical length scale. Different correlation strengths yield qualitatively similar dependence of λ upon bond portion, but λ at a fixed bond portion steadily increases with increasing correlation. This further affirms the idea that the size of a coherently deforming cluster becomes progressively larger with growing correlation. Results are shown in Fig. 4, panel (c), with trend lines computed from cubic basis splines.

We finally seek to account for the reentrant scaling of p_c with structural correlation strength by identifying the critical mechanical length scale, λ_c, at the onset of rigidity percolation for each structural correlation strength, c. We estimate λ_c by interpolation using the previously mentioned cubic basis splines. As shown in Fig. 4(d), we find that p_c varies nonmonotonically with λ_c, with an initial decrease until λ_c exceeds about five bond lengths, after which p_c once more increases. The optimal value of λ_c is that obtained for a

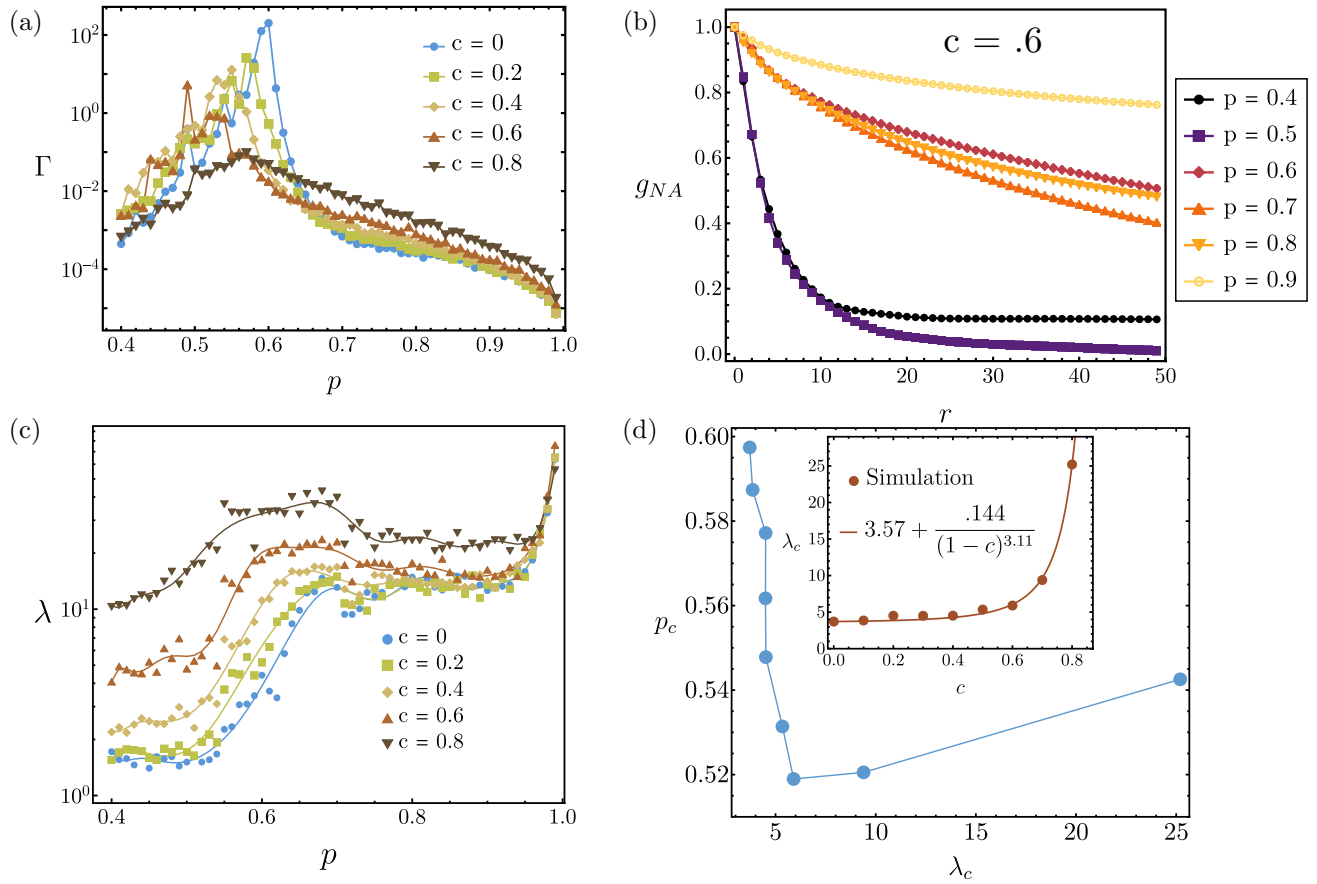

FIG. 4. (a) We show the nonaffine parameter, as defined in Eq. (6), vs bond portion for a number of correlation strengths. In each case, the nonaffine parameter exhibits a pronounced peak at the rigidity percolation transition. Larger correlation strengths correspond to nonaffine rearrangements occurring over a wider range of bond fractions and are reflected in the peaks becoming progressively broader with increasing c. (b) We display azimuthally averaged nonaffine correlations $g_{NA}(r)$ as a function of distance r between vertices. In each case, we find the decay to be exponential, allowing us to extract an emergent mechanical length scale, λ. This length scale monotonically increases with bond portion p, suggesting longer range correlations for networks with more fiber content. The nonaffine correlations in the large r limit decrease with increasing bond portion below the rigidity percolation threshold; however, above this threshold they increase with increasing bond portion. While we choose a correlation strength of 0.6 here, networks with differing correlation strength exhibited qualitatively similar behavior. Data are shown in symbols, while lines show the best fit to Eq. (8). In (c), we show emergent mechanical length scales λ for different combinations of p and c. At low bond portions, the length scale λ steadily increases with correlation strength for a given p, whereas at high bond portions, values of λ for different values of c converge and approach the system size. In (d), we identify a critical mechanical length scale, λ_c, as the decay length of nonaffine correlations at the onset of rigidity percolation, which exhibits a power law divergence as the structural correlation strength nears 1 (see inset). We show that the critical bond portion p_c varies nonmonotonically with λ_c in a manner reminiscent of the scaling of p_c with structural correlation strength c in Fig. 3(b).

structural correlation strength of 0.6, in concert with our previous findings. We further observe that λ_c appears to diverge according to a power law as c approaches 1. In the limit $c = 1$, either all bonds can be present or no bonds can be present, so that the only percolating network would be a fully connected network, in which vertex displacements are correlated over arbitrarily large distances. We thus find that, while small, rigid islands must nucleate to enable the most efficient percolation, excessively large rigid clusters leave too little material elsewhere to enable the formation of system-wide force chains.

IV. CONCLUSION

We have introduced and investigated a model of rigidity percolation in spatially correlated networks. Our study of the scaling of the shear modulus near percolation, coupled with our analysis of networks' strain fields, offers a straightforward physical picture accounting for the reentrant scaling of p_c with c. While the length scale over which a network's displacement field is well coordinated grows monotonically with correlation strength, eventually neighboring rigid clusters become poorly coupled. Weak tethers between dense islands of bonds lead to strain being highly concentrated, rather than the load being distributed evenly throughout the network.

This work broadens the already successful rigidity percolation framework to better account for the mechanical response of structurally correlated, heterogeneous networks found in cells and tissues. We anticipate this work will usher in further studies exploring the role of anisotropy [37] observed in many extracelluler matrices. Our findings indicate that, rather than using just an averaged, system-wide characterization of

network topology, local spatial patterns should be considered to fully understand tissues' responses to applied stress.

ACKNOWLEDGMENTS

The authors thank G. Koenderink, J. Schwarz, and J. Sethna for valuable discussions. This research was supported in part by the National Science Foundation Grants No. DMR-1808026, No. DMR-2118449, and No. DMR-1807602.

APPENDIX A: FINDING MECHANICAL GROUND STATES OF ELASTIC NETWORKS

We seek a zero-force configuration of the network, subject to the constraint that the nodes along the bottom of the network are fixed and the nodes along the top of the network do not translate in the y direction and are displaced by a uniform amount to the right. Periodic boundary conditions are imposed at the left and right boundaries of the network. We note that, due to the quadratic energy given by Eq. (2), the restoring force, $\vec{F}$, resulting from a displacement field $\vec{u}$ may be computed as

$$\vec{F} = -\mathbf{K}\vec{u}, \tag{A1}$$

where, for a network with N vertices, $\mathbf{K}$ is a $2N \times 2N$ matrix and $\vec{u}$ is a $(2N \times 1)$-dimensional column vector with the displacement field components of node i given in indices $2i - 1$ and $2i$ of $\vec{u}$. For a total energy E, the matrix element $K_{\alpha\beta}$ is given by

$$K_{\alpha\beta} = \frac{\partial^2 E}{\partial u_\alpha \partial u_\beta}, \tag{A2}$$

where $1 \leqslant \alpha, \beta \leqslant 2N$.

We then partition indices of the displacement field on the interval $[1, 2N]$ into two subsets: the set $\mathcal{R}$ of indices corresponding to relaxed coordinates and the set $\mathcal{B}$ of indices corresponding to constrained coordinates on the boundary. Let $\vec{u}_R$ be an $R \times 1$ column vector containing just those coordinates permitted to relax, where $R = |\mathcal{R}|$ is the number of relaxed coordinates. We further define a projection operator from the full $2N$-dimensional displacement field $\vec{u}$ to $\vec{u}_R$, denoted by $\mathbf{P}_{N\to R}$, and a projection operator $\mathbf{P}_{R\to N}$ from $\vec{u}_R$ back to $\mathbb{R}^{2N}$. The product $\mathbf{P}_{R\to N}\mathbf{P}_{N\to R}$ yields a $2N \times 2N$ linear operator satisfying

$$(\mathbf{P}_{R\to N}\mathbf{P}_{N\to R})_{\alpha\beta} = \begin{cases} 1, & \alpha = \beta,\ \alpha \in \mathcal{R}, \\ 0, & \text{otherwise.} \end{cases} \tag{A3}$$

Finally, we define a $2N \times 2N$ operator, $\mathbf{I}_B$, to select just those elements of $\vec{u}$ corresponding to boundary nodes' displacements:

$$I_{\alpha\beta} = \begin{cases} 1, & \alpha = \beta,\ \alpha \in \mathcal{B}, \\ 0, & \text{otherwise.} \end{cases} \tag{A4}$$

With the foregoing definitions in hand, we now return to the physical situation. The net force on the relaxed nodes due to interactions amongst relaxed nodes must be the opposite of the net force on relaxed nodes due to their interaction with

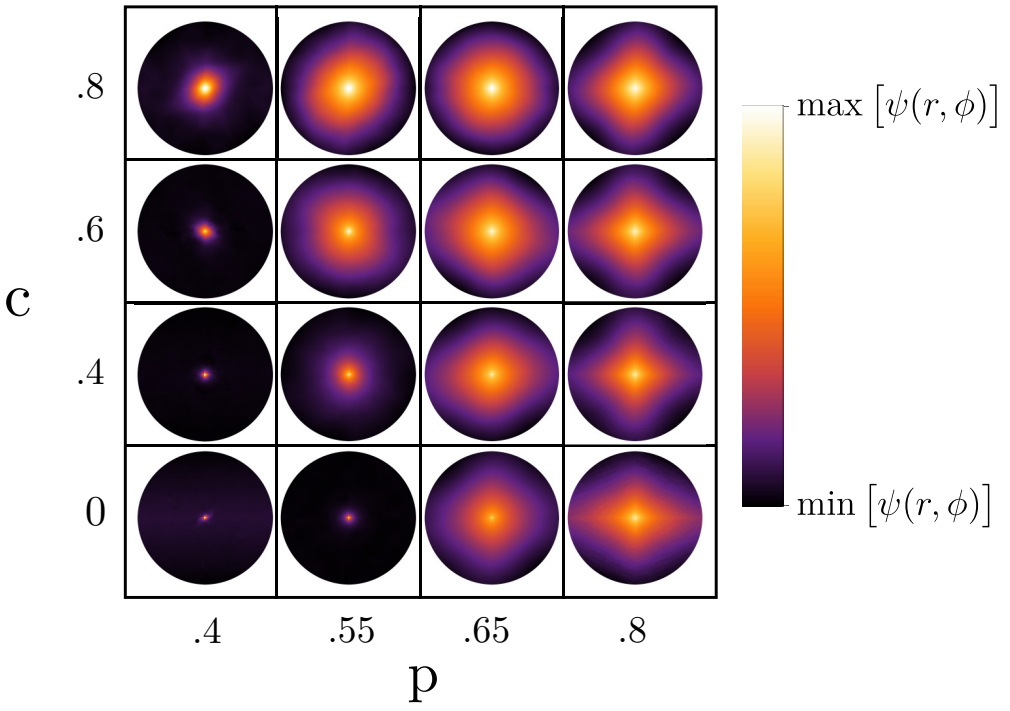

FIG. 5. We show the correlation in nonaffine parameter as a function of the magnitude and orientation of separation. The color scale for each panel is normalized to the maximum value for a given combination of bond portion and correlation strength. The decay in nonaffine displacement coefficient becomes more gradual with growing bond portion for all correlation strength, but growth in decay length becomes markedly more rapid for highly correlated networks. We also note that, with growing bond portion, nonaffine correlations exhibit increasing anisotropy, with decay in correlations becoming much more gradual along the direction of applied shear.

boundary nodes. In terms of the previously defined quantities, this implies

$$\mathbf{P}_{N\to R}\mathbf{K}\mathbf{P}_{R\to N}\vec{u}_R = -\mathbf{P}_{N\to R}\mathbf{K}\mathbf{I}_B\vec{u}. \tag{A5}$$

We choose as our starting guess the affine displacement field, $\vec{u}_A$, and decompose $\vec{u}$ as the sum of the affine field and the nonaffine field, $\vec{u}_{NA}$. Defining $\mathbf{K}_R \equiv \mathbf{P}_{N\to R}\mathbf{K}\mathbf{P}_{R\to N}$, we solve for the nonaffine component of $\vec{u}_R$, $\vec{u}_{NA,R}$ as

$$\vec{u}_{NA,R} = -\mathbf{K}_R^{+}(\mathbf{P}_{N\to R}\mathbf{K}\mathbf{I}_B\vec{u}_A + \mathbf{P}_{N\to R}\mathbf{K}\mathbf{P}_{R\to N}\vec{u}_{A,R}). \tag{A6}$$

$\mathbf{K}_R^{+}$ denotes the Moore-Penrose inverse of $\mathbf{K}_R$ [38–40], which we compute using the package SUITESPARSEQR [41]. We finally solve for the overall displacement field as

$$\vec{u} = \mathbf{P}_{R\to N}\vec{u}_{NA,R} + \vec{u}_A \tag{A7}$$

and the residual strain energy as

$$E = \frac{1}{2}\vec{u}^T\mathbf{K}\vec{u}. \tag{A8}$$

APPENDIX B: QUANTIFYING ANISOTROPY IN NONAFFINE CORRELATIONS

We further look for evidence of orientational order in nonaffine correlations by averaging not over an annular sector, but rather over all pairs of points whose relative displacement has magnitude r and makes an angle φ with the positive x axis. We define a measure of correlation $\psi(r,\varphi)$:

$$\psi(r,\phi) = \frac{\sum_{\vec{r}_1,\vec{r}_2}\vec{u}_{NA}(\vec{r}_1)\cdot\vec{u}_{NA}(\vec{r}_2)\delta_{r,|\vec{r}_1-\vec{r}_2|}\delta_{\varphi,\theta_{1,2}}}{\langle|\vec{u}_{NA}|^2\rangle\sum_{\vec{r}_1,\vec{r}_2}\delta_{r,|\vec{r}_1-\vec{r}_2|}\delta_{\varphi,\theta_{1,2}}}, \tag{B1}$$

where summations are over all vertices, δ is the Kronecker delta, and $\theta_{1,2}$ is the angle between the displacement $\vec{r}_2-\vec{r}_2$ and the positive x axis. Results are shown in Fig. 5. The color scale for each combination of correlation strength and bond portion is mapped to the range spanning the minimum and maximum values of ψ for that combination.

While, for low bond portions, the correlation between nonaffine displacement is highly isotropic, correlations decay far more gradually along the direction of applied strain at large bond portion. Well above the rigidity percolation threshold, networks deform in a nearly affine manner, as shown in Fig. 4(a). In this regime, the discrete rotational symmetry of the kagome network introduces elastic anisotropy. This anisotropy is more pronounced for networks with less structural correlation, as highly correlated networks have greater fluctuation in local stiffness, a trait known to increase nonaffinity [32]. Our analysis to elucidate the reentrance in the rigidity percolation threshold relies upon nonaffine correlations for $0.52 \leqslant p \leqslant 0.6$, where the nonazimuthally averaged nonaffine parameter decays nearly isotropically.

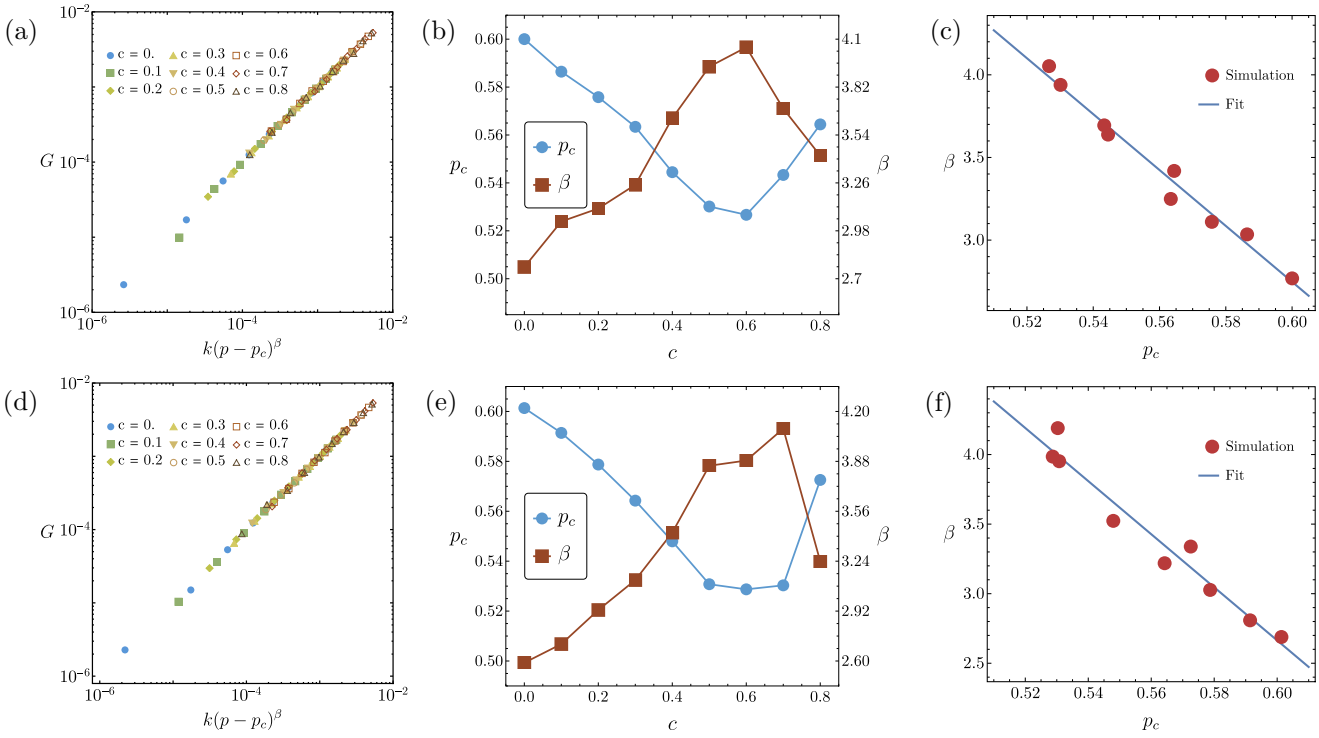

FIG. 6. We show the results of our study to check for finite size effects that may have influenced our findings. We show results for networks four times the size of those considered in the main text in panels (a)–(c) and results for networks 10 times the size of those considered in the main text in panels (d)–(f). In (a), we show agreement between simulation data and a fit to the exponential scaling model given by Eq. (5). In (b), we show the scaling of the critical bond portion and critical exponent with the correlation strength and find these results to be substantially similar to those shown in the main text, as shown in Fig. 3. In (c), we show the inverse relationship between the scaling exponent and the critical bond portion, once more finding our results in close accord with those presented previously. Panels (d)–(f) correspond with panels (a)–(c) and exhibit strong agreement with previous findings.

APPENDIX C: INVESTIGATING FINITE SIZE EFFECTS

As mentioned in the main text, we also sought to confirm that our findings remained valid for increasingly large networks. We considered cases in which the number of bonds in the fully connected state was ≈800 000 and ≈2 000 000. For each class, we varied the correlation strength c from 0 to 0.8, in steps of 0.1, and the bond portion, p, from 0.4 to 0.75, in steps of 0.01. We focused on the range from 0.45 to 0.7 for p as we were primarily interested in determining whether the same scaling behavior as reported in the main text occurred in the vicinity of the rigidity percolation transition.

We found that the scaling of the shear moduli of all larger networks was still well captured by Eq. (5) and further found the optimal correlation strength to be approximately 0.6. Values of scaling exponents for networks of different size but with the same correlation strength also proved to be strikingly similar, suggesting that our system size is indeed appropriate to reveal general bulk properties of structurally correlated fiber networks. A summary of our findings is provided in Fig. 6.

[1] *The Cytoskeleton*, edited by T. D. Pollard and R. D. Goldman (Cold Spring Harbor Laboratory Press, Cold Spring Harbor, NY, 2017).

[2] M. Gardel, J. Shin, F. MacKintosh, L. Mahadevan, P. Matsudaira, and D. Weitz, Elastic behavior of cross-linked and bundled actin networks, Science **304**, 1301 (2004).

[3] M. L. Gardel, J. H. Shin, F. C. MacKintosh, L. Mahadevan, P. A. Matsudaira, and D. A. Weitz, Scaling of F-Actin Network Rheology to Probe Single Filament Elasticity and Dynamics, Phys. Rev. Lett. **93**, 188102 (2004).

[4] M. Murrell, P. W. Oakes, M. Lenz, and M. Gardel, Forcing cells into shape: the mechanics of actomyosin contractility, Nat. Rev. Mol. Cell Biol. **16**, 486 (2015).

[5] G. Lee, G. Leech, M. J. Rust, M. Das, R. J. McGorty, J. L. Ross, and R. M. Robertson-Anderson, Myosin-driven actin-microtubule networks exhibit self-organized contractile dynamics, Sci. Adv. **7**, eabe4334 (2021).

[6] G. Lee, G. Leech, P. Lwin, J. Michel, C. Currie, M. J. Rust, J. L. Ross, R. J. McGorty, M. Das, and R. M. Robertson-Anderson, Active cytoskeletal composites display emergent tunable contractility and restructuring, Soft Matter **17**, 10765 (2021).

[7] S. Münster, L. M. Jawerth, B. A. Leslie, J. I. Weitz, B. Fabry, and D. A. Weitz, Strain history dependence of the nonlinear stress response of fibrin and collagen networks, Proc. Natl. Acad. Sci. USA **110**, 12197 (2013).

[8] J. L. Silverberg, A. R. Barrett, M. Das, P. B. Petersen, L. J. Bonassar, and I. Cohen, Structure-function relations and rigidity percolation in the shear properties of articular cartilage, Biophys. J. **107**, 1721 (2014).

[9] K. A. Jansen, A. J. Licup, A. Sharma, R. Rens, F. C. MacKintosh, and G. H. Koenderink, The role of network architecture in collagen mechanics, Biophys. J. **114**, 2665 (2018).

[10] F. Burla, C. Dussi, J. Martinez-Torres, J. Tauber, J. van der Gucht, and G. H. Koenderink, Connectivity and plasticity determine collagen network fracture, Proc. Natl. Acad. Sci. USA **117**, 8326 (2020).

[11] T. Wyse Jackson, J. A. Michel, P. Lwin, L. A. Fortier, M. Das, L. J. Bonassar, and I. Cohen, Structural origins of cartilage shear mechanics, Sci. Adv. **8**, eabk2805 (2022).

[12] N. I. Petridou, B. Corominas-Murta, C. Heisenberg, and E. Hannezo, Rigidity percolation uncovers a structural basis for embryonic tissue phase transitions, Cell **184**, 1914 (2021).

[13] C. D. DiDomenico, M. Lintz, and L. J. Bonassar, Molecular transport in articular cartilage - what have we learned from the last 50 years? Nat. Rev. Rheumatol. **14**, 393 (2018).

[14] S. Rhee, J. L. Puetzer, B. N. Mason, C. A. Reinhart-King, and L. J. Bonassar, 3d bioprinting of spatially heterogeneous collagen constructs for cartilage tissue engineering, ACS Biomater. Sci. Eng. **2**, 1800 (2016).

[15] S. Lalitha Sridhar, M. C. Schneider, S. Chu, G. de Roucy, S. J. Bryant, and F. J. Vernerey, Heterogeneity is key to hydrogel-based cartilage tissue regeneration, Soft Matter **13**, 4841 (2017).

[16] D. A. Head, A. J. Levine, and F. C. MacKintosh, Distinct regimes of elastic response and deformation modes of cross-linked cytoskeletal and semiflexible polymer networks, Phys. Rev. E **68**, 061907 (2003).

[17] J. Wilhelm and E. Frey, Elasticity of Stiff Polymer Networks, Phys. Rev. Lett. **91**, 108103 (2003).

[18] C. Heussinger and E. Frey, Floppy Modes and Nonaffine Deformations in Random Fiber Networks, Phys. Rev. Lett. **97**, 105501 (2006).

[19] M. Das, F. C. MacKintosh, and A. J. Levine, Effective Medium Theory of Semiflexible Filamentous Networks, Phys. Rev. Lett. **99**, 038101 (2007).

[20] E. M. Huisman, T. van Dillen, P. R. Onck, and E. Van der Giessen, Three-Dimensional Cross-Linked F-Actin Networks: Relation between Network Architecture and Mechanical Behavior, Phys. Rev. Lett. **99**, 208103 (2007).

[21] C. Broedersz, X. Mao, T. Lubensky, and F. C. MacKintosh, Criticality and isostaticity in fibre networks, Nat. Phys. **7**, 983 (2011).

[22] M. Das, D. A. Quint, and J. M. Schwarz, Redundancy and cooperativity in the mechanics of compositely crosslinked filamentous networks, PLoS One **7**, e35939 (2012).

[23] R. C. Picu, Mechanics of random fiber network a review, Soft Matter **7**, 6768 (2011).

[24] C. P. Broedersz and F. C. MacKintosh, Modeling semiflexible polymer networks, Rev. Mod. Phys. **86**, 995 (2014).

[25] S. Zhang, L. Zhang, M. Bouzid, D. Z. Rocklin, E. Del Gado, and X. Mao, Correlated Rigidity Percolation and Colloidal Gels, Phys. Rev. Lett. **123**, 058001 (2019).

[26] B. Ráth and A. Sapozhnikov, The effect of small quenched noise on connectivity properties of random interlacements, Elec. J. Prob. **2013**, 1 (2013).

[27] A. Zaccone, H. Wu, and E. Del Gado, Elasticity of Arrested Short-Ranged Attractive Colloids: Homogeneous and Heterogeneous Glasses, Phys. Rev. Lett. **103**, 208301 (2009).

[28] A. Weinrib and B. I. Halperin, Critical phenomena in systems with long-range-correlated quenched disorder, Phys. Rev. B **27**, 413 (1983).

[29] S. Feng, M. F. Thorpe, and E. Garboczi, Effective-medium theory of percolation on central-force elastic networks, Phys. Rev. B **31**, 276 (1985).

[30] C. Storm, J. J. Pastore, F. C. MacKintosh, T. C. Lubensky, and P. A. Janmey, Nonlinear elasticity in biological gels, Nature (London) **435**, 191 (2005).

[31] X. Mao, O. Stenull, and T. C. Lubensky, Elasticity of a filamentous kagome lattice, Phys. Rev. E **87**, 042602 (2013).

[32] B. A. DiDonna and T. C. Lubensky, Nonaffine correlations in random elastic media, Phys. Rev. E **72**, 066619 (2005).

[33] A. Zaccone and E. Scossa-Romano, Approximate analytical description of the nonaffine response of amorphous solids, Phys. Rev. B **83**, 184205 (2011).

[34] A. Zaccone and E. Terentjev, Short-range correlations control the g/k and poisson ratios of amorphous solids and metallic glasses, J. Appl. Phys. **115**, 033510 (2014).

[35] M. Mosayebi, P. Ilg, A. Widmer-Cooper, and E. Del Gado, Soft Modes and Nonaffine Rearrangements in the Inherent Structures of Supercooled Liquids, Phys. Rev. Lett. **112**, 105503 (2014).

[36] S. S. Schoenholz, A. J. Liu, R. A. Riggleman, and J. Rottler, Understanding Plastic Deformation in Thermal Glasses from Single-Soft-Spot Dynamics, Phys. Rev. X **4**, 031014 (2014).

[37] T. Zhang, J. M. Schwarz, and M. Das, Mechanics of anisotropic spring networks, Phys. Rev. E **90**, 062139 (2014).

[38] E. H. Moore, On the reciprocal of the general algebraic matrix, Bull. Am. Math. Soc. **26**, 394 (1920).

[39] A. Bjerhammar, Application of calculus of matrices to method of least squares: with special references to geodetic calculations, Trans. R. Inst. Tech. Stockholm **49** (1951).

[40] R. Penrose, A generalized inverse for matrices, Math. Proc. Cambr. Philos. Soc. **51**, 406 (1955).

[41] T. A. Davis, SuitesparseQR: Multifrontal multithreaded rank-revealing sparse QR factorization, ACM Trans. Math. Softw. **38**, 8 (2011).